

Low Temperature Reaction of Molecular Zinc Oxide Precursors in Ionic Liquids Leading to Ionogel Nanoparticles with Shape Anisotropy

Markus Voggenreiter,^[a] Pascal Vöpel,^[b] Bernd Smarsly,^[b] and Sebastian Polarz*^[a]

Keywords: Semiconductor oxides; Nanocrystal shape; Ionic liquids; Ionogels; Mesocrystals

Abstract. The majority of particle synthesis methods are based on nucleation and growth processes in solvents. Whereas the role of capping agents has been investigated extensively regarding control particle size and shape, the unique role of the solvent is understood to a much lesser extent. Compared to other polar solvents, e.g. water, ionic liquids (ILs) are unique because their properties can be fine-tuned precisely by appropriate choice and modification of cation and anion. This makes ILs also interesting for particle synthesis. We present the generation of zinc oxide (ZnO) in imidazolium ILs starting from mo-

lecular precursors. A hydrolytic, sol-gel based synthesis route is suitable to achieve nanocrystalline ZnO. We find by in-situ synchrotron wide angle X-ray diffraction that in ILs an unusual ZnO phase with α -boron nitride structure acts as an intermediate prior to crystallization of the thermodynamically stable Wurtzite. This special mechanism leads to organic-inorganic hybrid IL/ZnO nanoparticles with plate-like morphology. Because of the large content of IL embedded in the ZnO matrix the novel particles gain ionogel properties, e.g. ion conductivity probed by impedance spectroscopy.

Introduction

Nanoparticle research has become an area of research of enormous importance.^[1] A change in properties compared to the bulk can be observed for almost any material, either because confinement influences the electronic system, because of a large surface to volume ratio or a special surface chemistry. This and the recent interest in the preparation of particle superstructures is one reason,^[2] why there is a steadily increasing interest in particles with a controlled shape.^[1a,3]

The well-known quantum size effect gives high relevance to nanoparticles made from semiconductors. Among semiconductors certain metal oxides like titanium dioxide (TiO₂) or zinc oxide (ZnO) have shown to be of high relevance, which can also be seen from the large number of articles and reviews on these two materials.^[4] Both components contain abundant and cheap elements, they are non-toxic and stable in air. They are produced at the multi-ton scale as pigments, in rubber vulcanization, as catalyst supports or in UV protection. They also gained relevance in modern applications like for photovoltaic cells, photocatalysts or sensors, and in most of these cases the nanoparticle character of the materials is relevant. ZnO, unlike TiO₂, is a direct gap semiconductor, which leads to some additional, valuable features.^[5]

The latter argument is one of the reasons, why we became interested in zinc oxide several years ago. We could establish a very effective, molecular system $[R^1ZnOR^2]_4$ as a single-source precursor for zinc oxide.^[6] ZnO can be obtained in nanocrystalline form either by thermal treatment at moderate temperatures (≈ 200 – 250 °C) or via a hydrolytic route offering the advantages of sol-gel chemistry at temperatures close to ambient. A notable advantage of the mentioned precursor system is that with choosing different groups $R^1 = \text{Me, Et}$ and $R^2 = \text{Et, isoPr, tertBu}$. OEtOMe reaction kinetics for ZnO formation can be adjusted on the molecular scale.

One of the most frequent methods for nanoparticle synthesis starts from a homogeneous solution of ions or precursors.^[7] By adjusting conditions or the adding reactants nucleation and growth is initiated. Capping agents or surfactants are used to control growth and to prevent agglomeration. The solvent is typically regarded just as a “beholder”, which only insignificantly influences nanoparticle genesis.^[8] The question how the solvent manipulates the growth of particles is difficult to answer, also because it is hard to find a materials source which is soluble in different solvents. E.g. salts, which are used frequently for the preparation of metal oxides, are well soluble in water, but one cannot use them in apolar, organic media.

However, with ionic liquids (ILs) one has highly polar solvents with organic character in stock, and ILs have also been used in the literature for nanoparticle synthesis.^[9] A small number of papers have already applied ionic liquids for the preparation of ZnO materials.^[10] We want to investigate if the aforementioned ZnO precursor chemistry can be transferred to ILs as a solvent, and if, for nanoparticles synthesis, special phenomena can be observed. First, we check if the thermal or the hydrolytic route is more suitable for ZnO nanoparticle

* Prof. Dr. S. Polarz
E-Mail: sebastian.polarz@uni-konstanz.de

[a] University of Konstanz
Universitätsstrasse 10
78457 Konstanz, Germany

[b] Department of Chemistry
Justus-Liebig Universität Giessen
Heinrich-Buff-Ring 17
35392 Giessen, Germany

Supporting information for this article is available on the WWW under <http://dx.doi.org/10.1002/zaac.201600341> or from the author.

generation. Next, we investigate the structure of the particles and their formation mechanism in detail. Finally, relevant functional properties of the materials as solid electrolytes are reported.

Results and Discussion

Identification of Precursors and Thermal Decomposition Route

First, it makes sense to check the compatibility of $[R^1ZnOR^2]_4$ precursors with ionic liquids as a solvent. Because of their good commercial availability, we have selected imidazolium-based ILs as solvents for the current study.^[11] This system grants a high variability considering systematic variation of the alkyl-chain attached to the imidazolium ring and different available anions. On the precursor side, keeping $R^1 = Me$ fixed, a series of compounds can be prepared with $R^2 = Me$ (1), Et (2), *iso*Pr (3), Bn (4), EtOMe (5), (EtO)₂Me (6), (EtO)₃Me (7), and EtO*iso*Pr(OMe)₂ (8) by reacting $ZnMe_2$ with the respective alcohol (see Chart 1). The synthesis was checked by NMR spectroscopy and comparison to spectroscopic data from the literature and our own, past work (see Supporting Information S1). A ZnO material prepared from, for instance, $[MeZnO*iso*Pr]_4$ as a precursor and butylmethyl-imidazolium acetate will be termed ZnO-3bi in the following.

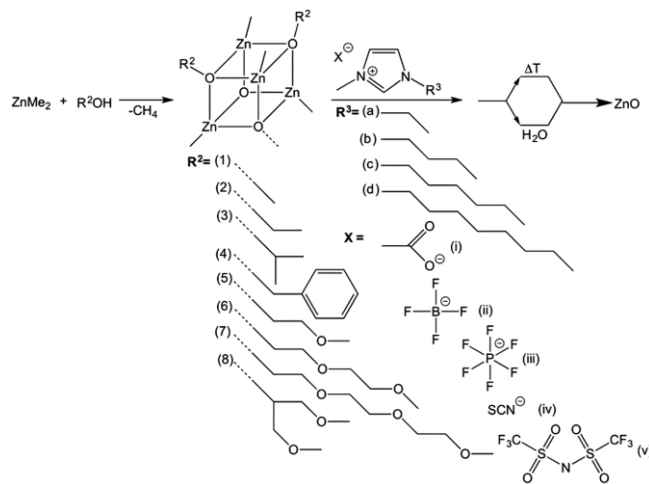


Chart 1. Overview of molecular precursors and ILs, and route from precursor to zinc oxide.

IL and the precursor were mixed and the suspension was filtered. From NMR spectra taken from the solution, we obtained a first impression about the amount of dissolved precursor. As an independent technique, we also used thermogravimetric analysis under oxygen. One can calculate the amount of precursor that had been dissolved in the IL by quantification of the mass of the remaining ZnO. The substituents in the precursor have major impact on their solubility in the IL. More hydrophobic compounds (1–3) hardly dissolve. In the case of precursor (4), the remaining mass of ZnO after TGA treatment (see Figure 1a) is 1.5%, which means that $q = m(\text{precursor})/$

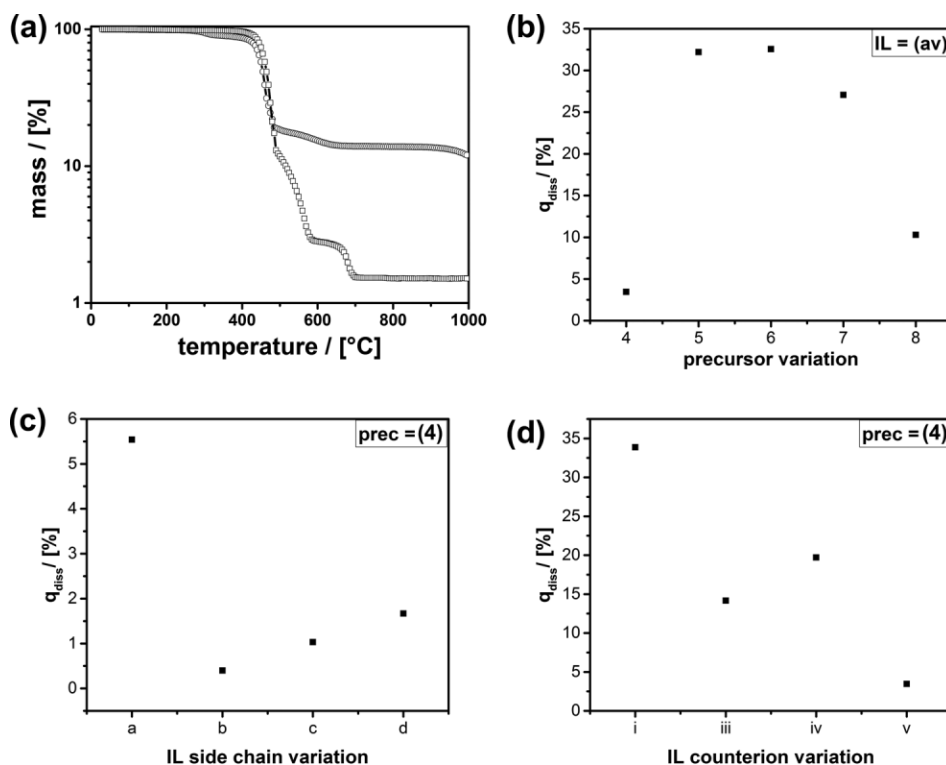


Figure 1. (a) TGA analysis in air for precursor (4; squares) and (5; circles) dissolved in IL (av). (b) Solubility in IL (av) for different precursors. (c) Solubility depending on the length of the substituent attached to the imidazolium ring. (d) Solubility depending on the type of counterion.

$m(\text{IL}) = 3.5\%$ had been dissolved. The solubility could be increased further, when the substituents of the precursor contain polar groups as in the cases (5–8). E.g., a solution containing $q = 32\%$ of precursor (as deduced from TGA shown in Figure 1a, b) could be obtained using compound (5). Also the length of the alkyl-chain attached to the imidazolium ring (Figure 1c) influences solubility. Precursor (4) was used as a model case. As expected, solubility increases, when the IL itself becomes more hydrophobic with longer alkyl chains. However, it is surprising that (4) exhibits best solubility in IL (av) with the shortest alkyl-chain. A hypothesis could be that the shorter chains allow some π - π interactions between the imidazolium and the benzene ring. The IL counterion has an influence as well as shown in Figure 1d. Obviously, the ability for coordination is a deciding factor. Acetate, which can coordinate to Zn^{2+} , leads to very high solubility. Less coordinating IL anions [e.g. BTA (v)] reduce the solubility. This section can be summarized as follows: By adjusting the molecular architecture of both the IL and the precursor one can obtain even highly concentrated solutions. The precursors are sufficiently soluble for the following materials synthesis attempts.

Therefore, we tested next, if thermal decomposition of the precursor dissolved in the IL would lead to ZnO and eventually to colloidal nanoparticles. It can also be proven by TGA that thermal decomposition of the ZnO precursors is typically taking place in the temperature range $\approx 250\text{ }^\circ\text{C}$ (see Supporting Information S2).^[6d] Because the thermal stability of ILs can be as high as $400\text{ }^\circ\text{C}$, it is expected that the thermal route should be feasible. Although ZnO in the thermodynamically stable Wurtzite modification has formed, as proven by powder X-ray diffraction (PXRD), one also sees that the material is very impure (Figure 2). The black coloration indicates the ma-

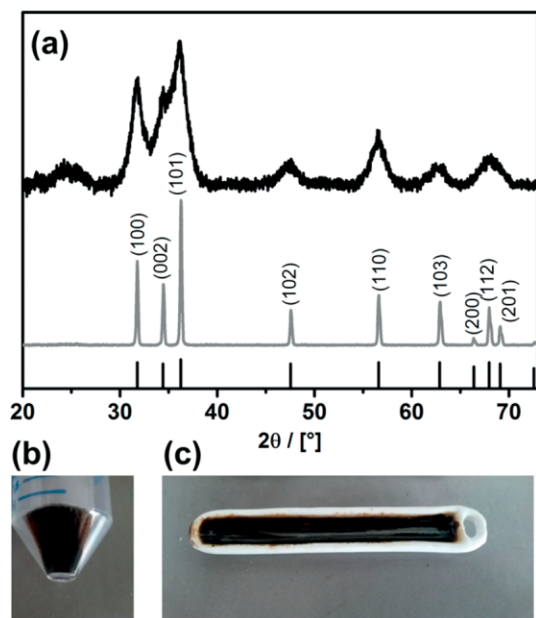


Figure 2. (a) PXRD pattern of ZnO-5bv as prepared ($T_{\text{reaction}} = 200\text{ }^\circ\text{C}$; black curve) and after high-T treatment ($T_{\text{sinter}} = 1000\text{ }^\circ\text{C}$; grey curve). The reference pattern of Wurtzite-ZnO is also shown (black bars at the bottom). Photographic images of ZnO-5bv as-prepared (b) and after high-T treatment (c).

terial contains significant amount of carbon, which cannot be removed even after high-T treatment. Unfortunately, it becomes evident that the thermal route is not suitable for the preparation of defined ZnO nanomaterials in ILs. The formation of carbon is not so surprising because others, for instance Antonietti et al., have very successfully used ILs as precursors for the preparation of various interesting carbon materials.^[12] Because in the current work, we are not focusing on potential ZnO/carbon composite materials, we do not follow this route further.

Hydrolytic, Sol-gel Chemistry in ILs

As an alternative to the thermal procedure described before, we tried if a hydrolytic route is more promising (see also Chart 1). It is important to note that water is used here as a reagent and not as a solvent. Ultimately all water is consumed in course of the reaction. As a reference experiment, the precursor was converted hydrolytically into ZnO using an alternative solvent (acetone or tetrahydrofuran) under otherwise identical conditions. The PXRD pattern of the prepared sample is shown in Figure 3a. Mainly one can see only the scattering of the sample holder. Only at $2\theta \approx 36^\circ$ there is a shoulder corresponding to a very broad signal in the range, where one would expect the most intense peaks of Wurtzite ZnO. Therefore, it can be concluded that only an amorphous product was

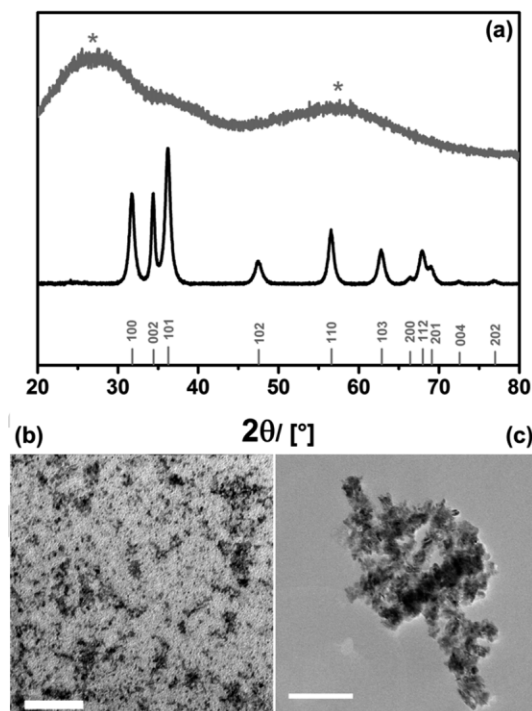


Figure 3. (a) PXRD pattern of ZnO prepared without IL as a reference (grey) and ZnO-5bii (black). The pattern of ZnO-Wurtzite is also shown (grey bars). Background scattering from the sample holder is marked with (*). TEM micrographs of amorphous ZnO formed in the presence of an IL (b) and nanocrystalline ZnO formed in the presence of an IL (c). Scale bars $\approx 100\text{ nm}$. For ZnO-5bii measured at higher magnification see Supporting Information S3.

prepared, which is in good agreement to our previous results about growth in organic solvents published by us in 2008.^[6c] The finding of an amorphous phase fits to transmission electron microscopy (TEM) data shown in Figure 3b. Only, ill-defined agglomerates of very small particles are seen.

When the IL is present during synthesis (Figure 3a; ZnO-5bii), one can clearly identify the set of signals characteristic for Wurtzite ZnO. In agreement to this, in TEM larger particles are present. From images taken at larger magnification (see Supporting Information S3) it also becomes clear that those particles are crystalline. However, particle size and shape does not seem to be much defined.

The mechanism of ZnO formation was investigated in further detail by in-situ PXRD using high-intensity synchrotron radiation. The results are shown in Figure 4a. Surprisingly, early in the reaction, besides the expected signals for Wurtzite-ZnO, a signal at $q = 22.9 \text{ nm}^{-1}$ corresponding to a lattice spacing of 0.27 nm is most intense. This signal fits to an alternative ZnO polymorph with α -boron nitride (α -BN) structure found by us in 2010.^[6f] In the meantime the phase could be confirmed by others, and theoretical reports support its existence. With time one sees the BN-ZnO signal disappears and the W-ZnO signals become more and more pronounced. This indi-

cates that the BN-ZnO is a direct precursor state for the thermodynamically stable zinc oxide phase (Wurtzite).^[13] Because such a sequence has not been found in other solvents yet, it seems a special feature of ILs is to at least partially stabilize the α -BN-ZnO modification. The latter hypothesis can be confirmed by lowering the reaction temperature ($T = 0 \text{ }^\circ\text{C}$), and, thus, lowering the conversion rate to the thermodynamically stable W-ZnO.

In PXRD (Figure 4d) signals for W-ZnO are absent, and the pure BN-ZnO phase seems to be present. However, closer inspection reveals that all signals with c component are missing, which is only consistent with a strict 2D growth of one BN-ZnO layer. It should be noted, that also for other (semi-)conductor materials 2D forms are observed and are in the focus of current international research, most prominently graphite \rightarrow graphene.^[14] It can be concluded ILs have a high tendency to stabilize the [002] lattice plane of ZnO, and this gives preference to 2D growth stabilizing the BN modification. The 2D, sheet-like character is nicely confirmed by TEM micrographs shown in Figure 4e. However, also the α -BN form should not be the center of the current paper. Nevertheless, one should keep in mind ILs can be used to stimulate 2D growth of ZnO nanostructures.

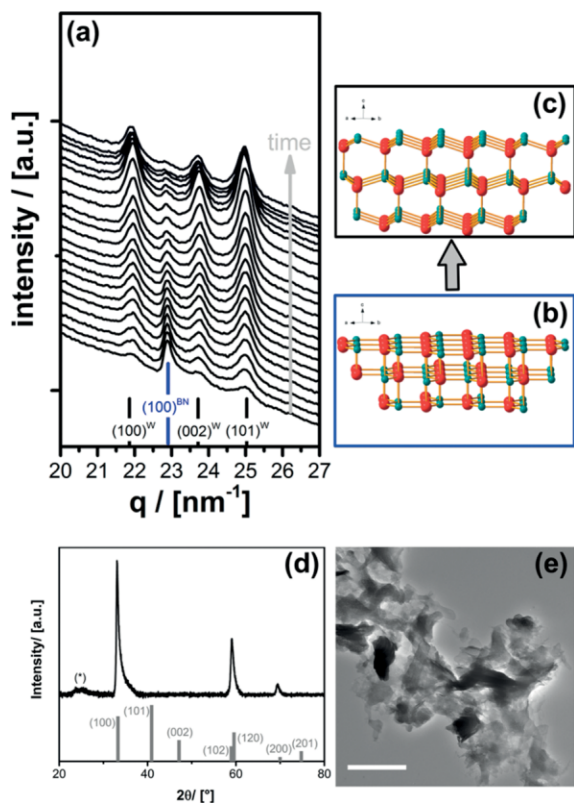


Figure 4. (a) Time-dependent, in-situ synchrotron PXRD measurements for the formation of ZnO in ILs (bv) by the hydrolytic conversion of molecular precursors (4). The reference signals for Wurtzite-ZnO (W) are shown as black bars and of α -BN ZnO (BN) in blue. The crystal structures of the α -BN ZnO (b) and Wurtzite-ZnO (W) (c) are also given. Zinc atoms are grey; oxygen atoms are red. PXRD pattern (d; * marks a signal from the sample holder) and TEM micrograph (e; scalebar 500 nm) of α -BN ZnO prepared in IL at $0 \text{ }^\circ\text{C}$.

Growth Control and Ionogel Nanoparticles

Our next task is to study how the ZnO nanocrystal shape can be controlled. First, we tested, if the choice of the IL anion had an influence, and as an analytical tool we have mainly applied PXRD (Figure 5a). This is possible, because in the PXRD pattern one finds signals with crystallographic a, b component only, for instance the (100), which contain information about the extension of the nanocrystals in a and b direction considering the intensity and width of the peaks. Quantitative information can be obtained from full profile analysis of the

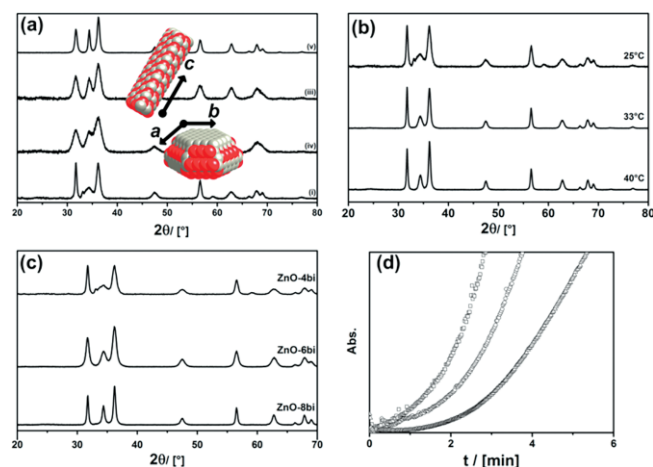


Figure 5. (a) PXRD patterns of ZnO-5b materials with a systematic variation of the IL anion. (b) PXRD patterns for ZnO-5bi samples prepared at three different temperatures. (c) PXRD pattern for a variation of the precursor while keeping the IL (bi) constant. (d) Time dependent absorption data ($\lambda = 320 \text{ nm}$) for the reaction of precursor (8) with water (squares), (6; circles) and (4; triangles).

PXRD data. On the other hand, the (002) signal tells about the growth of the nanocrystals in *c* direction.

We find an increasing coordinating character of the anion leads to a restricted growth of the particles in *c* direction as seen from the reduced intensity and increased width of the (002) signal in Figure 5a. Crystallites in ZnO-5bv with the low coordinating BTA anion have rod-like morphology with an aspect ratio $dc/da,b = 1.6$ (dc is the extension of the nanocrystal in *c* direction). The aspect ratio (0.3) of particles prepared using acetate as an anion (ZnO-5bi) is characteristic for a nanoplate morphology. The observed effect can be explained by the polar character of the Wurtzite crystal structure. The *c* axis is the polar axis, and thus without stabilization the [002] lattice plane (e.g. composed only of Zn^{2+}) has rather high energy. Consequently, ZnO has a natural preference for growth in *c* direction. However, when coordinating agents are present, they can bind to the [002] lattice plane, stabilizing such surfaces.^[15] Eventually, those surface are partially passivated, and growth takes place preferentially in *a,b* direction. The assumption that the described kinetic factors are important for the growth of the nanoparticles can be confirmed by studying the influence of temperature (Figure 5b). At higher temperatures, when the reaction rate speeds up, the (002) signal becomes slightly sharper, and this indicates that there is now a little more growth in *c* direction.

We also checked, if the alky-chain attached to the imidazolium ring has any influence on the shape of the nanocrystals, but this was not the case (see Supporting Information S4). On the other hand, the reaction kinetics of the precursor regarding hydrolysis and formation of ZnO has a significant influence (Figure 5c). With a bandgap of $E = 3.3$ eV bulk ZnO develops an adsorption edge at $\lambda = 390$ nm. Due to the quantum-size effect, for small nanoparticles as in the case here, there is a blue-shift to smaller wavelengths. Nevertheless, one can now follow the formation of ZnO using in-situ UV/Vis spectroscopy at a fixed wavelength (e.g. $\lambda = 320$ nm; see also Supporting Information S5). The measured absorption values can be plotted as a function of time (Figure 5d) revealing information about the respective reaction rate. In the shown series precursor (8) reacts fastest, and this leads to a notable growth in *c* direction as seen from the (002) signal in PXRD (Figure 5d). The precursor reacting slowest (4) gives rise to the ZnO particles with the most pronounced nanoplate morphology ($q = 0.2$). Indeed, in TEM and scanning electron (SEM) micrographs shown in Figure 6 one observes plate-like particles.

In addition to PXRD and the hexagonal cross-section also the lattice planes appearing in HRTEM (Figure 6c; for a larger image see Supporting Information Figure S6) indicate that the particles are crystalline. Final proof is given by electron diffraction (ED) as shown in Figure 6e. The diffraction pattern is characteristic for Wurtzite-ZnO with only one crystal domain. The orientation of the particle in the electron beam was perpendicular to the crystallographic *c* axis. Thus, the main growth direction is in *a,b* direction, which is consistent with the aforementioned studies by PXRD (see Figure 5).

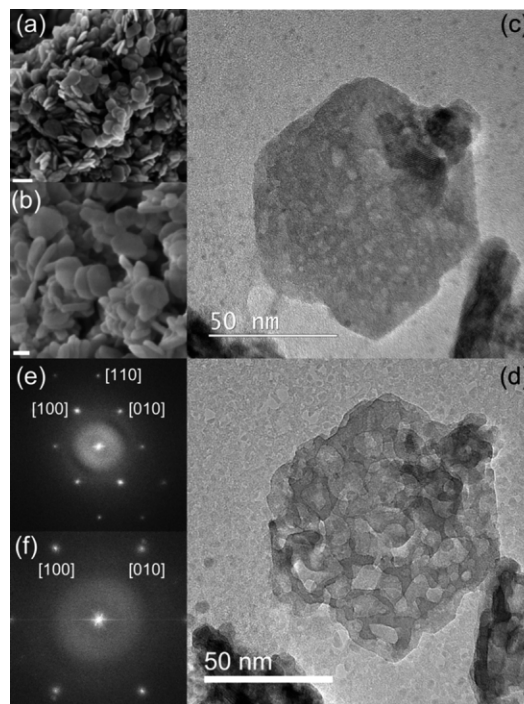


Figure 6. SEM micrographs of ZnO-4bi (a; scalebar = 100 nm), (b; scalebar = 40 nm). TEM micrograph (c,d) and ED (e,f) of one individual, hexagonal particles before and after longer exposure to the electron beam.

However, there are several inconsistencies. Most obvious is that the particles are extremely sensitive against the electron beam (see Figure 6c and d). For crystalline ZnO particles such sensitivity is not known. Particles containing significant amount of organic constituents are often not stable in the electron beam, which is a first indication that this is not pure ZnO. Big vacancies are rapidly “etched” into the particles, giving them an interesting nanostructure. The remaining particle, according to ED (Figure 6f), is still containing ZnO with the same crystallographic orientation. Some further factors are unusual. The size of the hexagonal nanoplates is obviously in the range 50–100 nm (*a,b* direction). In SEM, for particles lying in another orientation, one can estimate the thickness (*c* direction) to be 10–15 nm (see Supporting Information Figure S7). These values are in disagreement with particles extensions obtained from PXRD via peak width analysis ($D_{a,b} \approx 15$ nm; $D_c \approx 4$ –5 nm). Therefore, from PXRD one would have expected smaller particles than actually seen in TEM. Our conclusion is that the particles seen in TEM are not pure ZnO. TGA measurements of ZnO-5bi and ZnO-5bii are given in Figure 7a.

Both materials contain significant amounts of volatile constituents ($\Delta m = 17.5\%$; 12.3%). The temperatures of the main mass-loss determined from the first derivative of the TGA data ($T = 281$ °C and $T = 352$ °C) correlate well with the decomposition temperatures of the pure ILs (see also Supporting Information, Figure S8). The assumption that the materials and, thus also the particles, contain significant amount of IL is confirmed by IR measurements shown in Figure 7b. All characteristic vibrations of IL (bi) are present in ZnO-5bi. There is a

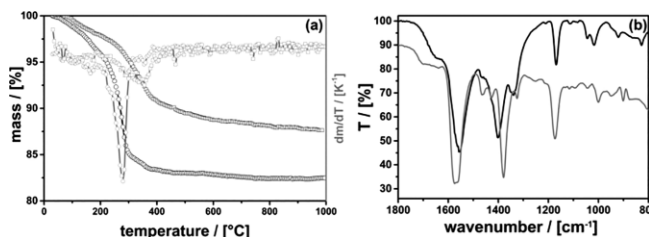


Figure 7. (a) TGA (black) and first derivative (grey) of ZnO-5bi (circles) and ZnO-5bii (squares). (b) FT-IR spectra of pure IL (bi) as a reference and of ZnO-bi.

small shift in the wavenumber of the carboxy group (1570, 1380 cm⁻¹) and of the imidazolium ring (1173 cm⁻¹), which can be explained by a notable interaction of the anion and the cation of the IL with the metal oxide surfaces. That there is a high tendency for the binding of ILs to metal oxides fits to other observations reported in the literature.^[16] Considering that the density of ZnO is 5.61 g·cm⁻³ and of IL (bi) only 1.005 g·cm⁻³ means that for a material with 17.5 mass-% IL roughly 50% of its volume is actually the IL. This value fits nicely to the impression we get from Figure 6d.

Organic-inorganic hybrids between high content of ILs and metal oxides are known in the literature with silica as the inorganic constituent as so-called ionogels.^[17] The silica forms a gel-like, solid matrix, and the IL is confined in the pores of this gel. To the best of our knowledge neither ZnO ionogels nor ionogel nanoparticles have been reported in the literature yet.^[18] One of the advantageous properties of ionogels is that they can be applied as a solid ion-conductor material.^[19] If the materials presented in the current study truly have ionogel characteristics, we also have to expect ion conductivity. An appropriate method to study ion conductivity of solid materials is impedance spectroscopy.^[20] The Nyquist plot of a representative case (ZnO-4bi) is shown in Figure 8a. Compared to the pure IL (Figure 8b) all materials prepared in the current study have a lower ionic conductivity, which is not surprising since the materials are not anymore liquids but solids. However, for ZnO-5bii, which contains rod-like ZnO nanocrystals the slope of temperature dependent data is almost the same than for the pure IL. This shows that the mechanism of ion conduction is presumably very similar. For the plate-like, hexagonal ionogel nanoparticles the initial ionic conductivity is roughly two orders of magnitude lower, which can be explained by the

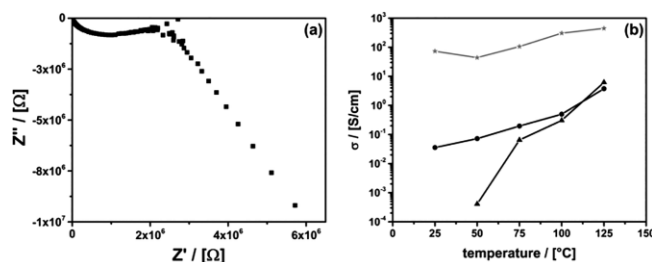
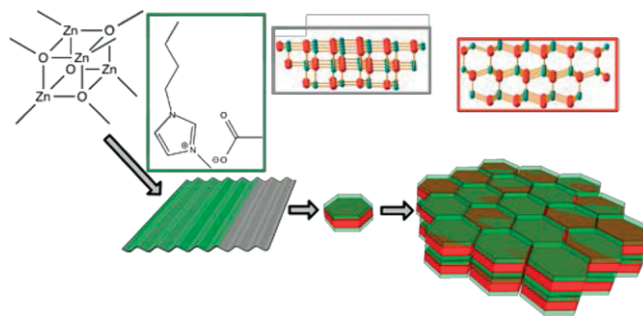


Figure 8. (a) Impedance spectrum (Nyquist plot) for ZnO-4bi. (b) Temperature dependency of ionic conductivity for pure IL (bi) (grey stars) as a reference, ZnO-5bii (black circles) and ZnO-4bi (black triangles).

stronger attachment of the IL to the surfaces. However, it is remarkable that the slope of the temperature dependent data is much larger. Because the slope is connected to the activation barrier of ionic transport this can be seen as a clear sign, that the special nano-architecture presented herein leads to a new mechanism of ion movement.

Conclusions

Summarizing the insights achieved up to this point, we can postulate a formation mechanism for the ionogel nanoparticles (see Scheme 1). The hydrolytic conversion of the molecular precursors in the presence an imidazolium-based IL is kinetically controlled. Instead of the thermodynamically stable Wurtzite modification ZnO forms in the form of the α-BN modification. A key for the stabilization of α-BN ZnO and the preference for 2D growth in crystallographic *a,b* direction is the strong interaction of the IL (cation and anion) with the surfaces of the inorganic matrix. Then, transformation into the more stable W-ZnO takes place, but significant amount of IL remains attached to the [002] surfaces. One can imagine that this process results in primary nanocrystals with an anisotropic surface chemistry: Organic and hydrophobic, where the IL is located, and inorganic and polar, at the sides. A secondary structure can now form by self-assembly of the small nanocrystals via oriented attachment, leading to larger particles with ionogel-character. The generation of such larger supracrystals by oriented attachment is in line with the literature for other organic-inorganic hybrid particles.^[21] Ultimately, when every nanocrystal is in a defined position in space, such superstructures have also been named mesocrystals.^[22] It could be shown that the mesocrystals achieved in the current state represent solid electrolyte in the form of nanocrystals.



Scheme 1. Formation mechanism of IL-ZnO hybrid nanocrystals with ionogel properties.

Experimental Section

Chemicals: Starting compounds were purchased from Sigma Aldrich and Iolitec. Solvents were dried prior to use with common procedures. Ionic liquids were dried under vacuum at 80 °C for 10 h. All reactions were performed using Schlenk technique.

Preparation of ZnO precursor [MeZnOR]₄: The organometallic precursors were prepared according to a previously published procedure

by reacting the desired alcohol with dimethylzinc.^[6c] Because of the pyrophoric nature of dimethylzinc special caution should be adopted.

Thermal Decomposition of ZnO-Precursor: [MeZnOEtOMe]₄ (0.1 mL) precursor was mixed with ionic liquid (1 mL). The mixture was transferred in a ceramic-ship and treated in a tube furnace in a nitrogen or oxygen flow (0.2 L·min⁻¹) at 200 °C for 1 h. Nanoparticles were collected by centrifugation (10000 rpm) and washed 2 times with 5 mL acetone.

Preparation of ZnO-IL Nanoparticles: ZnO precursor (0.13 mmol) was dissolved in ionic liquid (1 mmol). For decreasing the viscosity of the solvent small amounts of acetone can be added. The initiation of the sol-gel process took places with the injection of H₂O (0.3 mL). The mixture was stirred at room temperature for 3 h. Nanoparticles were isolated by centrifugation (9000 rpm) and washed 2 times with acetone (5 mL).

In-situ WAXS/SAXS Measurements: In-situ WAXS/SAXS analyses were done at Beamline 5.2 in Elettra Synchrotron Facility (Trieste, Italy). The monochromatic wavelength of the beam was 0.077 nm and the used energy 16 keV. The data was obtained by using a WAXS detector Pilatus 100 k and a SAXS detector Pilatus3 1 M. Reactions were done in glas-capillaries from Hilgenberg GmbH (80 mm × 15 mm) with a thickness of 0.1 mm. WAXS/SAXS measurements were carried out in-situ and time resolved with a resolution of 1 pattern per minute.

Characterization: X-ray diffractions were performed with a Bruker AXS D8 Advance diffractometer using Cu-K_α radiation. Particle sizes were determined by using topas-software and Debye-Scherrer (Le-Bail-Fit). UV-VIS-Kinetic measurements were done with a Varian Cary 50 scan UV/Vis spectrophotometer. FT-IR spectra were obtained with a Perkin-Elmer Spectrum 100 with ATR measurement unit. TGA-measurements were performed with a STA (Simultane Thermo Analyse) Modell 429 from Netzsch. ¹H and ¹³C NMR spectra were obtained with a Bruker 400 MHz spectrometer and the software Mestrenova. (HR)-TEM images were acquired with a JEOL, JEM 2200FS at an accelerating voltage of 200 kV. SEM images were acquired with a Zeiss Crossbeam IS40XB instrument operating at 4 kV. Impedance spectroscopy measurements to determine the ionic conductivity were performed with a Zahner IM6. The amplitude was set to 50 mV and the frequency range of 1 Hz to 1 MHz was used.

Supporting Information (see footnote on the first page of this article): S-1. Molecular characterization of precursors. S-2. Thermal properties of precursors. S-3. TEM of ZnO5bii. S-4. Variation of alkyl chain. S-5. In-situ UV/Vis data. S-6. HRTEM of ZnO4bi. S-7. SEM data of nanoplates. S-8. TGA of pure ILs.

Acknowledgements

We thank the Deutsche Forschungsgemeinschaft (DFG) for funding of the project within the framework of the SPP 1708 (Materials Synthesis Near Room Temperature). We also thank the SFB-1214 (Anisotropic Particles as Building Blocks) for the possibility to use the Particle Analysis Centre for nanoparticle characterization.

References

- [1] a) C. Burda, X. B. Chen, R. Narayanan, M. A. El-Sayed, *Chem. Rev.* **2005**, *105*, 1025–1102; b) M. C. Daniel, D. Astruc, *Chem. Rev.* **2004**, *104*, 293–346; c) A. H. Lu, E. L. Salabas, F. Schuth, *Angew. Chem. Int. Ed.* **2007**, *46*, 1222–1244.
- [2] a) C. L. Chen, N. L. Rosi, *Angew. Chem. Int. Ed.* **2010**, *49*, 1924–1942; b) Y. Gao, Z. Y. Tang, *Small* **2011**, *7*, 2133–2146.
- [3] S. Polarz, *Adv. Funct. Mater.* **2011**, *21*, 3214–3230.
- [4] a) X. Chen, S. S. Mao, *Chem. Rev.* **2007**, *107*, 2891–2959; b) U. Ozgur, Y. Alivov, C. Liu, A. Teke, M. A. Reshchikov, S. Dogan, V. Avrutin, S. J. Cho, H. Morkoc, *J. Appl. Phys.* **2005**, *98*, 103; c) Z. L. Wang, *J. Phys.: Condens. Matter* **2004**, *16*, R829–R858; d) C. Pacholski, A. Kornowski, H. Weller, *Angew. Chem. Int. Ed.* **2002**, *41*, 1188.
- [5] a) M. H. Huang, S. Mao, H. Feick, H. Q. Yan, Y. Y. Wu, H. Kind, E. Weber, P. Russo, P. D. Yang, *Science* **2001**, *292*, 1897–1899; b) Q. F. Zhang, C. Dandeneau, X. Y. Zhou, G. Z. Cao, *Adv. Mater.* **2009**, *21*, 4087–4108.
- [6] a) S. Polarz, F. Neues, M. W. E. van den Berg, W. Grunert, L. Khodeir, *J. Am. Chem. Soc.* **2005**, *127*, 12028–12034; b) S. Polarz, A. V. Orlov, F. Schuth, A. H. Lu, *Chem. Eur. J.* **2007**, *13*, 592–597; c) C. Lizandara-Pueyo, M. W. E. van den Berg, A. De Toni, T. Goes, S. Polarz, *J. Am. Chem. Soc.* **2008**, *130*, 16601–16610; d) V. Ischenko, S. Polarz, D. Grote, V. Stavarache, K. Fink, M. Driess, *Adv. Funct. Mater.* **2005**, *15*, 1945–1954; e) C. Lizandara-Pueyo, S. Siroky, M. R. Wagner, A. Hoffmann, J. S. Reparaz, M. Lehmann, S. Polarz, *Adv. Funct. Mater.* **2011**, *21*, 295–304; f) C. L. Pueyo, S. Siroky, S. Landsmann, M. W. E. van den Berg, M. R. Wagner, J. S. Reparaz, A. Hoffmann, S. Polarz, *Chem. Mater.* **2010**, *22*, 4263–4270.
- [7] a) C. B. Murray, C. R. Kagan, M. G. Bawendi, *Annu. Rev. Mater. Sci.* **2000**, *30*, 545–610; b) J. Park, K. J. An, Y. S. Hwang, J. G. Park, H. J. Noh, J. Y. Kim, J. H. Park, N. M. Hwang, T. Hyeon, *Nat. Mater.* **2004**, *3*, 891–895.
- [8] a) J. P. Cason, M. E. Miller, J. B. Thompson, C. B. Roberts, *J. Phys. Chem. B* **2001**, *105*, 2297–2302; b) M. Niederberger, G. Garnweitner, *Chem. Eur. J.* **2006**, *12*, 7282–7302.
- [9] a) M. Antonietti, D. B. Kuang, B. Smarsly, Z. Yong, *Angew. Chem. Int. Ed.* **2004**, *43*, 4988–4992; b) H. Itoh, K. Naka, Y. Chujo, *J. Am. Chem. Soc.* **2004**, *126*, 3026–3027.
- [10] a) X. Zhou, Z. X. Xie, Z. Y. Jiang, Q. Kuang, S. H. Zhang, T. Xu, R. B. Huang, L. S. Zheng, *Chem. Commun.* **2005**, 5572–5574; b) J. Wang, J. M. Cao, B. Q. Fang, P. Lu, S. G. Deng, H. Y. Wang, *Mater. Lett.* **2005**, *59*, 1405–1408; c) T. Alammari, A. V. Mudring, *Mater. Lett.* **2009**, *63*, 732–735; d) I. Yavari, A. R. Mahjoub, E. Kowsari, M. Movahedi, *J. Nanopart. Res.* **2009**, *11*, 861–868.
- [11] T. Welton, *Chem. Rev.* **1999**, *99*, 2071–2083.
- [12] J. P. Paraknowitsch, J. Zhang, D. S. Su, A. Thomas, M. Antonietti, *Adv. Mater.* **2010**, *22*, 87.
- [13] a) B. Rakshit, P. Mahadevan, *Phys. Rev. Lett.* **2011**, *107*, 4; b) D. Zagorac, J. C. Schon, M. Jansen, *J. Phys. Chem. C* **2012**, *116*, 16726–16739; c) D. Gebauer, H. Colfen, *Nano Today* **2011**, *6*, 564–584.
- [14] S. Z. Butler, S. M. Hollen, L. Y. Cao, Y. Cui, J. A. Gupta, H. R. Gutierrez, T. F. Heinz, S. S. Hong, J. X. Huang, A. F. Ismach, E. Johnston-Halperin, M. Kuno, V. V. Plashnitsa, R. D. Robinson, R. S. Ruoff, S. Salahuddin, J. Shan, L. Shi, M. G. Spencer, M. Terrones, W. Windl, J. E. Goldberger, *ACS Nano* **2013**, *7*, 2898–2926.
- [15] C. Lizandara-Pueyo, M. C. Morant-Minana, M. Wessig, M. Krumm, S. Mecking, S. Polarz, *RSC Adv.* **2012**, *2*, 5298–5306.
- [16] S. Schernich, M. Laurin, Y. Lykhach, N. Tsud, M. Sobota, T. Skala, K. C. Prince, N. Taccardi, V. Wagner, H. P. Steinruck, V. Matolin, P. Wasserscheid, J. Libuda, *ChemPhysChem* **2013**, *14*, 3673–3677.
- [17] a) J. Le Bideau, L. Viau, A. Vioux, *Chem. Soc. Rev.* **2011**, *40*, 907–925; b) M. A. Neouze, J. Le Bideau, P. Gaveau, S. Bellayer, A. Vioux, *Chem. Mater.* **2006**, *18*, 3931–3936.
- [18] a) Y. Mei, Y. Lu, B. Yan, *J. Photochem. Photobiol. A: Chem.* **2014**, *280*, 1–4; b) S. Thiemann, S. J. Sachnov, F. Pettersson, R. Bollstrom, R. Osterbacka, P. Wasserscheid, J. Zaumseil, *Adv. Funct. Mater.* **2014**, *24*, 625–634.

- [19] a) T. Echelmeyer, H. W. Meyer, L. van Wullen, *Chem. Mater.* **2009**, *21*, 2280–2285; b) J. Le Bideau, J. B. Ducros, P. Soudan, D. Guyomard, *Adv. Funct. Mater.* **2011**, *21*, 4073–4078.
- [20] I. M. Hodge, M. D. Ingram, A. R. West, *J. Electroanal. Chem.* **1976**, *74*, 125–143.
- [21] a) Y. Yin, A. P. Alivisatos, *Nature* **2005**, *437*, 664–670; b) K. S. Cho, D. V. Talapin, W. Gaschler, C. B. Murray, *J. Am. Chem. Soc.* **2005**, *127*, 7140–7147.
- [22] a) H. Colfen, M. Antonietti, *Angew. Chem. Int. Ed.* **2005**, *44*, 5576–5591; b) R. Q. Song, H. Colfen, *Adv. Mater.* **2010**, *22*, 1301–1330.

Received: September 18, 2016
Published Online: ■

*M. Voggenreiter, P. Vöpel, B. Smarsly, S. Polarz** **1–9**

Low Temperature Reaction of Molecular Zinc Oxide Precursors in Ionic Liquids Leading to Ionogel Nanoparticles with Shape Anisotropy

